Investigation of the spin state of Co in $LaCoO_3$ at room temperature: *Ab initio* calculations and high-resolution photoemission spectroscopy of single crystals

S. K. Pandey,[1,4] Ashwani Kumar,[2] S. Patil,[1] V. R. R. Medicherla,[1] R. S. Singh,[1] K. Maiti,[1]
D. Prabhakaran,[3] A. T. Boothroyd,[3] and A. V. Pimpale[4]
[1]*Department of Condensed Matter Physics and Materials Science, Tata Institute of Fundamental Research, Homi Bhabha Road, Colaba, Mumbai 400 005, India*
[2]*Department of Physics, Institute of Science and Laboratory Education, IPS Academy, Indore 452 012, India*
[3]*Clarendon Laboratory, Department of Physics, University of Oxford, Parks Road, Oxford OX1 3PU, United Kingdom*
[4]*UGC-DAE Consortium for Scientific Research, University Campus, Khandwa Road, Indore 452 017, India*
(Received 3 July 2007; revised manuscript received 18 September 2007; published 18 January 2008)

We investigate the spin state of $LaCoO_3$ using state-of-the-art photoemission spectroscopy and *ab initio* band structure calculations. The GGA+U calculations provide a good description of the ground state for the experimentally estimated value of electron correlation strength U. In addition to the correlation effect, spin-orbit interaction is observed to play a significant role in the case of intermediate spin and high spin configurations. The comparison of the calculated Co $3d$ and O $2p$ partial density of states with the experimental valence band spectra indicates that at room temperature, Co has dominant intermediate spin state configuration and that the contribution from high spin configuration may not be significant at this temperature. The line shape of the La $5p$ and O $2s$ core level spectra could be reproduced well within these *ab initio* calculations.

DOI: 10.1103/PhysRevB.77.045123 PACS number(s): 71.20.−b, 75.20.Hr, 71.27.+a, 79.60.Bm

I. INTRODUCTION

The evolution of the spin state of Co in $LaCoO_3$ with temperature has drawn a great deal of attention during the last 50 years.[1–10] The ground state of this compound is believed to be a nonmagnetic (spin $S=0$) insulator. It shows two magnetic transitions at about 100 K (a sharp transition) and at around 500 K (broad).[11] The second transition is also accompanied by an insulator to metal transition. All these magnetic transitions have been attributed to the temperature induced spin state transition of Co^{3+} ions. Initially, it was believed that the transition at 100 K occurs due to the change in the spin state of Co^{3+} ions from a low spin (LS) state ($t_{2g}^6 e_g^0 \Rightarrow S=0$) to mixed LS and high spin (HS) states ($t_{2g}^4 e_g^2 \Rightarrow S=2$).[1,3] In order to achieve a microscopic understanding of these transitions, photoemission spectroscopy (PES) and x-ray absorption spectroscopy (XAS) have been employed extensively since these techniques help to probe the electronic structure directly.[6–8] The experimental results were simulated using configuration interaction calculations for the cluster of CoO_6 octahedron. All these investigations inferred the presence of varying mixtures of LS and HS states above 100 K.

Subsequently, a detailed study[9] based on LDA+U (LDA=local density approximation and U=electron-electron Coulomb repulsion strength) calculations attributed the 100 K transitions to LS to orbital ordered intermediate spin (IS) state ($t_{2g}^5 e_g^1 \Rightarrow S=1$) and the one at 500 K to orbital disordered IS state as the energy of the latter state was found to be higher than the former and lower than the HS state. Since then, numerous experimental and theoretical works have been carried out, which attributed the first transition to LS to the IS state.[12–18] This has also been demonstrated by PES and XAS studies,[19] where Co $2p$ core level, valence band, and O K-edge XAS spectra of $LaCoO_3$ revealed 70% LS and 30% IS states in the temperature range of 100–300 K. No contribution of HS state was observed up to 300 K.

Recently, based on GGA+U (GGA=generalized gradient approximation) calculations, Knízek *et al.* showed that the mixed LS-HS state (1:1) is the first excited state and thus attributed the first magnetic transition from LS to LS-HS state.[20] This is in sharp contrast to the belief of IS contributions in the intermediate temperature range. In addition, experimental results based on XAS and magnetic circular dichroism[21] and inelastic neutron scattering[22] are also interpreted in terms of mixed LS-HS state in the temperature range up to 700 K considering cluster approximations. It is thus evident that the spin state of Co at different temperatures is still controversial.

In this work, we investigate the spin state of Co in $LaCoO_3$ at room temperature using state-of-the-art photoemission spectroscopy and *ab initio* band structure calculations. We observe that spin-orbit coupling (SOC) plays an important role in determining the electronic structure in this system. The comparison of the high-resolution spectra and the calculated results suggest that the electronic structure of $LaCoO_3$ at room temperature has large IS contributions. The *ab initio* calculations also provide a good representation of the experimental La $5p$ and O $2s$ core level spectra.

II. EXPERIMENTAL AND COMPUTATIONAL DETAILS

Single crystal of $LaCoO_3$ was grown and characterized as described elsewhere.[23] The photoemission spectra of the valence band and shallow core levels were recorded at room temperature (RT) using a spectrometer equipped with monochromatic Al $K\alpha$ (1486.6 eV) and He I (21.2 eV) sources and a Gammadata Scienta analyzer, SES2002. The base pressure during the measurements was about 4×10^{-11} Torr. The energy resolution for the x-ray photoemission was set to 0.3 eV for the valence band and 0.6 eV for the core level spectra. The resolution for the He I spectrum was fixed to

4 meV. The sample was cleaned *in situ* by scraping the sample surface using a diamond file. The cleanliness of the sample was ascertained by tracking the sharpness of the O 1*s* peak and the absence of C 1*s* peak. The Fermi level was aligned by recording the valence band spectrum of a Ag foil mounted on the same sample holder.

The LDA+U, GGA+U (U represents the electron correlation strength among Co 3*d* electrons) and spin-polarized density of states (DOS) calculations were carried out using LMTART 6.61.[24] For calculating charge density, full-potential linearized muffin-tin orbital (LMTO) method working in plane wave representation was employed. In the calculation, we have used the muffin-tin radii of 3.515, 2.005, and 1.64 a.u. for La, Co, and O, respectively. The charge density and effective potential were expanded in spherical harmonics up to $l=6$ inside the sphere and in a Fourier series in the interstitial region. The initial basis set included 6*s*, 5*p*, 5*d*, and 4*f* valence and 5*s* semicore orbitals of La, 4*s*, 4*p*, and 3*d* valence and 3*p* semicore orbitals of Co, and 2*s* and 2*p* orbitals of O. The exchange correlation functional of the density functional theory was taken after Vosko *et al.*[25] and GGA calculations are performed following Perdew *et al.*[26]

In GGA+U calculations, the Coulomb interaction U and the exchange interaction strength J among various electrons are normally used. In order to minimize uncertainty due to large number of parameters, we have used only two parameters: $U=3.5$ eV and $J=1$ eV among Co 3*d* electrons. The calculations were performed by taking LS, IS, and HS configurations, which correspond to $(t_{2g\uparrow}^3 t_{2g\downarrow}^3)$, $(t_{2g\uparrow}^3 t_{2g\downarrow}^2 e_{g\uparrow}^1)$, and $(t_{2g\uparrow}^3 t_{2g\downarrow}^1 e_{g\uparrow}^2)$ electronic configurations, respectively, as the initial input. It is to note here that while the calculations within LDA search for the ground state, in LDA+U method, there are several stable solutions corresponding to different local minima as also observed by Korotin *et al.*[9] Therefore, these calculations enable to capture solutions corresponding to different initial spin configurations.

To simulate the room temperature electronic structure, we have used the lattice parameters corresponding to the crystal structure at room temperature. In order to calculate the DOS corresponding to high temperature phase, the lattice parameters at the corresponding temperature have been used in various studies and it has already been shown that such consideration provides a good description of the electronic structure at different temperatures.[9,16] Self-consistency was achieved by demanding the convergence of the total energy to be smaller than 10^{-4} Ry/cell. Final orbital occupancies for Co t_{2g} and e_g states were obtained from self-consistent GGA+U calculations for different initial state configurations. (8,8,6) divisions of the Brillouin zone along three directions for the tetrahedron integration were used to calculate the DOS.

III. RESULTS AND DISCUSSIONS

It is well known that although the electron correlation effects are underestimated in *ab initio* band structure calculations within LDA, these results are often found to explain most of the features in PES and XAS results in transition metal oxide systems.[27–31] However, one needs to consider the correlation effects to capture the details of the spectra and the ground state properties of the system. We have calculated various contributions in the DOS of $LaCoO_3$ using both LDA and LDA+U methods. In order to minimize uncertainty in the calculated results, we have fixed the value of U to the experimentally estimated values of 3.5 eV.[32]

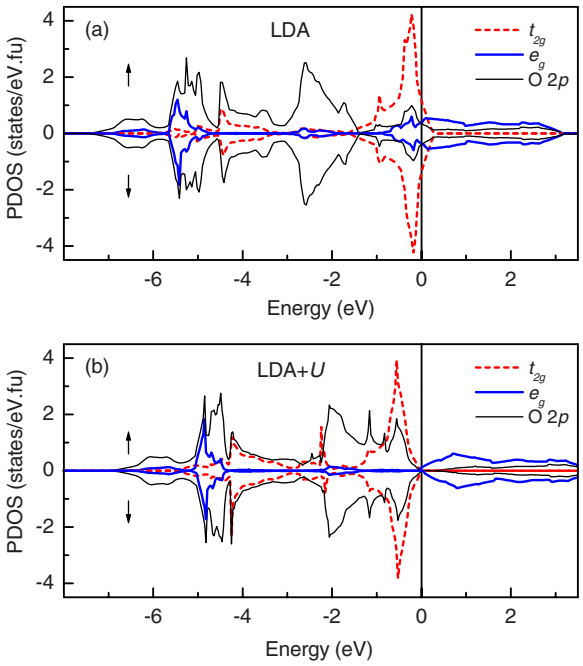

FIG. 1. (Color online) O 2*p* (thin solid line) and Co 3*d* partial densities of states having t_{2g} (dashed line) and e_g (thick solid line) symmetries from (a) LDA and (b) LDA+U calculations.

In Fig. 1(a), we show the calculated LDA results for both the up and down spin states. There are several features observed in different energy positions. The features between −1.5 and −3 eV energies are dominated by the O 2*p* states with negligible contribution from other electronic states. These features are identified as O 2*p* nonbonding states. The features at lower energies have dominant contributions from O 2*p* electronic states with small but finite intensities from the Co 3*d* states having t_{2g} and e_g symmetries. Thus, the features between −3 and −4.5 eV can be attributed to bonding states with t_{2g} symmetry and those below −4.5 eV are the bonding states with e_g symmetry. The antibonding features appear above −1.5 eV and have a predominantly Co 3*d* character. Co 3*d* bands with t_{2g} symmetry appear between −1.5 and 0.5 eV and the e_g bands between −1 and 3 eV. It is evident that the density of states at the Fermi level is large, suggesting a metallic phase in the ground state in contrast to the insulating phase observed in various experiments.

The effect of electron correlation in the density of states is manifested in the LDA+U results, as shown in Fig. 1(b). Although electron correlation among O 2*p* electrons is not considered in the calculations, the energy distribution of the O 2*p* partial density of states (PDOS) appears to be somewhat different from the LDA results. The O 2*p* contribution in the antibonding region appears to be enhanced in the LDA+U results compared to the LDA results, suggesting a spectral weight transfer from the bands having bonding char-

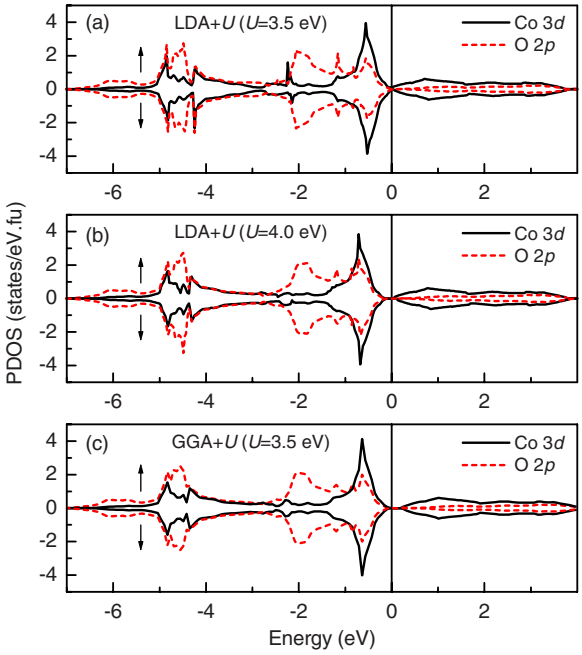

FIG. 2. (Color online) Co 3*d* and O 2*p* partial densities of states calculated using (a) LDA+*U* (*U*=3.5 eV), (b) LDA+*U* (*U* =4 eV), and (c) GGA+*U* (*U*=3.5 eV) methods.

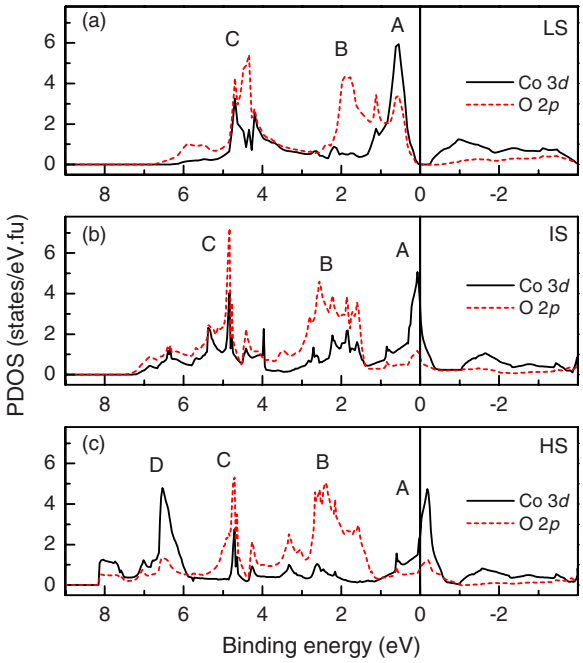

FIG. 3. (Color online) Calculated Co 3*d* and O 2*p* partial densities of states corresponding to low spin (LS), intermediate spin (IS), and high spin (HS) configurations using the GGA+*U* method.

acter. The nonbonding O 2*p* contributions also shift toward the Fermi level. The changes in the Co 3*d* bands are most significant as expected. The bonding and antibonding e_g bands shift toward higher energies. The bonding t_{2g} band appears almost at the same energies along with a significant increase in the spectral weight. Subsequently, the antibonding t_{2g} band having primarily Co 3*d* character becomes narrower along with a reduction in spectral weight. It is thus clear that consideration of *U* in the calculations leads to a decrease in Co 3*d* character and an increase in O 2*p* character of the bands in the vicinity of the Fermi level. Although the overlap between the t_{2g} and e_g bands is minimized for these parameters, no hard gap is observed characterizing the systems to be metallic.

In order to investigate the value of *U* that creates a gap at the Fermi level, we compare the Co 3*d* and O 2*p* PDOSs for *U*=3.5 eV and 4 eV in Figs. 2(a) and 2(b), respectively. It is evident that an increase in *U* to 4 eV generates a band gap of about 0.2 eV. The shape and energy distribution of the DOS is almost the same in both the cases. The GGA is known to provide a better description of the exchange-correlation functional as it also considers first order correction to the spatial distribution of the electronic charge density used in the LDA calculations. In GGA, the total energy of the system improves[26] and it is expected that the energy position of different bands would also improve. The calculated PDOSs of Co 3*d* and O 2*p* corresponding to GGA+*U* calculations are shown in Fig. 2(c). In contrast to the metallic phase observed in LDA results, a value of *U*=3.5 eV creates a band gap of about 0.22 eV at the Fermi level in the results corresponding to GGA calculations, which is very close to that observed experimentally.[33,34] However, the shape and positions of Co 3*d* and O 2*p* bands are very similar in the LDA+*U* and GGA+*U* results. Thus, we used the GGA+*U* method in the remaining part of our study to discuss the experimental results.

We now turn to the question of the influence of various spin states in the electronic structure of $LaCoO_3$. The PDOSs obtained for different spin state configurations are shown in Fig. 3 for the same values of *U* (=3.5 eV). It is evident that although the LS configuration leads to an insulating ground state, the electronic structure corresponding to IS and HS configurations converges to a metallic phase. This is a well known fact for this system and one needs to consider additional parameters such as orbital ordering to achieve an insulating phase.[9] However, the energy distribution of the DOS over the large binding energy scale remains very similar. There are three distinctly separable features A, B, and C in the DOS in Fig. 3. In the case of IS configuration, the t_{2g} band becomes partially filled. This effect enhances further in the case of HS configuration. The total intensity of feature A gradually decreases with the change in spin state configuration from LS→IS→HS. In addition, the Co 3*d* character of feature A becomes highest in the IS configuration (80.3%), while it is about 63.8% in the LS state and 64.8% in the HS state. Feature B representing the nonbonding O 2*p* states appears at slightly higher binding energies in the IS and HS states compared to that in the LS state. The change in feature C is again substantial. The O 2*p* and Co 3*d* contributions are almost similar in LS and IS cases. In the case of HS states, feature C has a dominant O 2*p* character and a new feature D having a dominant Co 3*d* character appears beyond 6 eV binding energies.

All the above calculations are done without considering the SOC in any of the electronic states. Recently, there is a growing realization that SOC plays a crucial role in deter-

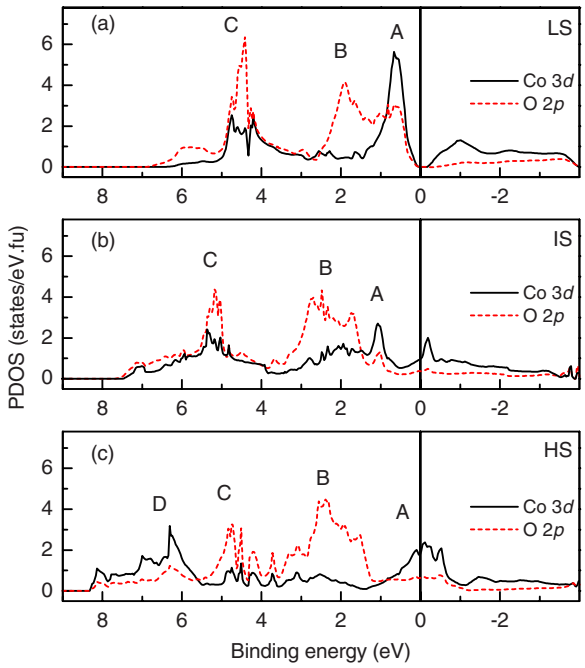

FIG. 4. (Color online) Co 3*d* and O 2*p* partial densities of states corresponding to low spin (LS), intermediate spin (IS), and high spin (HS) configurations calculated including spin-orbit interactions. All these calculations are performed using the GGA+*U* method.

mining the electronic structure in various transition metal oxides. The importance of SOC has been demonstrated in the systems possessing rare-earth 4*f* electrons.[35] In Ca_2RuO_4, it was shown that SOC plays an important role in the change-over of the spin and orbital anisotropy as a function of temperature.[36] Very recent theoretical studies of Ca_3CoRhO_6 compound have shown that the insulating ground state can be achieved by considering SOC in the calculations.[37] In order to investigate the effect in the present case, we have calculated the PDOS in all the cases including SOC. The results are shown in Fig. 4. It is clear that SOC has no significant influence in the case of LS configuration. This is presumably due to the fact that all the energy bands are completely filled. The effect is most pronounced in Fig. 4(b) corresponding to the IS state exhibiting a splitting of the sharp feature A.

The effects of spin-orbit coupling in the occupancies of $t_{2g\uparrow}$, $e_{g\uparrow}$, $t_{2g\downarrow}$, and $e_{g\downarrow}$ are given in Table I. Numbers written in normal and boldface correspond to without SOC and with SOC, respectively. The total electronic occupancies of Co 3*d* bands corresponding to LS, IS, and HS states are about 6.7, 6.65, and 6.47, respectively. These values are closer to those obtained from full-multiplet configuration interaction calculations carried out by Saitoh *et al.*[19] and somewhat smaller from those obtained by Korotin *et al.*[9] It is evident that the total occupancies as well as partial occupancies of t_{2g} and e_g orbitals corresponding to LS and HS states are not affected significantly by SOC. However, in the IS state, the occupancies of $e_{g\uparrow}$ orbitals decrease by 0.14 and those of $t_{2g\downarrow}$ orbital increase by 0.08 due to the spin-orbit coupling keeping the total occupancy almost unchanged.

TABLE I. Occupancies of different Co 3*d* orbitals obtained from GGA+*U* calculations for low spin (LS), intermediate spin (IS), and high spin (HS) configurations of Co^{3+} in $LaCoO_3$. Numbers written in normal and boldface correspond to calculation without spin-orbit coupling and with spin-orbit coupling, respectively.

Initial spin state	$t_{2g\uparrow}$	$e_{g\uparrow}$	$t_{2g\downarrow}$	$e_{g\downarrow}$	Total
LS	2.77	0.58	2.77	0.58	6.7
	2.77	**0.59**	**2.77**	**0.58**	**6.71**
IS	2.79	1.5	1.95	0.43	6.67
	2.8	**1.36**	**2.03**	**0.45**	**6.64**
HS	2.82	1.9	1.32	0.42	6.46
	2.83	**1.9**	**1.35**	**0.41**	**6.49**

The details of the effect of SOC in the IS state are shown in Fig. 5, where we show the up and down spin PDOSs of Co 3*d* bands separately. In Fig. 5(a), the feature in the vicinity of the Fermi level arises due to the down spin t_{2g} states. This feature splits into two distinctly separated features (the energy separation is about 1.2 eV). The feature at about 1 eV binding energy represents the doubly degenerate d_{xz} and d_{yz} bands and the nondegenerate d_{xy} band appears above the Fermi level. The doubly degenerate bonding $e_{g\uparrow}$ band also splits by about 1 eV into $d_{x^2-y^2}$ and d_{z^2} bands, as shown in the inset of Fig. 5(b). It is thus clear that the degeneracy in the t_{2g} and e_g bands are partially lifted due to spin-orbit interactions and the effect is most pronounced in the IS configuration. Since the *d* bands are not completely filled, the splitting of the t_{2g} and e_g bands will influence the occupancy

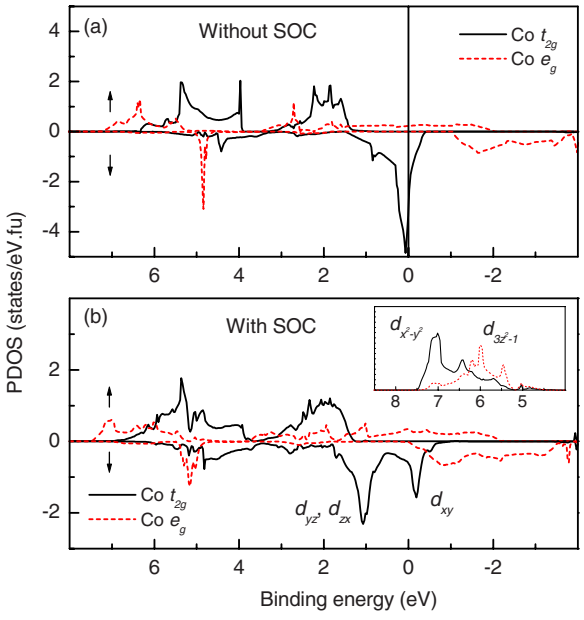

FIG. 5. (Color online) Spin-polarized partial density of states corresponding to Co t_{2g} and e_g bands calculated (a) without spin-orbit coupling and (b) with spin-orbit coupling. The inset shows $d_{x^2-y^2}$ and d_{z^2} contributions in the $e_{g\uparrow}$ band.

TABLE II. Occupancies of 3*d* orbitals in intermediate spin configuration of Co^{3+} in $LaCoO_3$. Numbers written in normal and boldface correspond to calculation without spin-orbit coupling and with spin-orbit coupling, respectively.

Spin	d_{yz}	d_{xz}	d_{xy}	$d_{x^2-y^2}$	d_{z^2}
Up	0.93	0.93	0.93	0.75	0.75
	0.93	**0.93**	**0.94**	**0.86**	**0.50**
Down	0.65	0.65	0.65	0.21	0.21
	0.92	**0.92**	**0.19**	**0.22**	**0.23**

of these bands. Here, the SOC induced splitting leads to the decrease in energy of d_{yz}, d_{zx}, and $d_{x^2-y^2}$ bands and enhances the energy of d_{xy} and d_{z^2} bands. Thus, the occupancies of d_{yz}, d_{zx}, and $d_{x^2-y^2}$ are expected to increase and those of d_{xy} and d_{z^2} to decrease. This is clearly manifested in the partial occupancies of each Co 3*d* orbitals given in Table II, where the occupancies of $d_{yz\downarrow}$, $d_{zx\downarrow}$, and $d_{(x^2-y^2)\uparrow}$ increase by 0.27, 0.27, and 0.11, respectively, and those of $d_{xy\downarrow}$ and $d_{z^2\uparrow}$ decrease by 0.46 and 0.15, respectively.

In order to compare the calculated results with the experimental spectra, we show the background subtracted experimental valence band spectra at RT in Fig. 6. The spectra show three distinct features at about 1.0, 2.9, and 5.3 eV binding energies denoted by A, B, and C, respectively. The relative intensity of various features are significantly different in the spectra using Al $K\alpha$ and He I sources. While feature A is the most intense in the Al $K\alpha$ spectrum, it becomes the weakest in intensity in the He I spectrum. Subsequently,

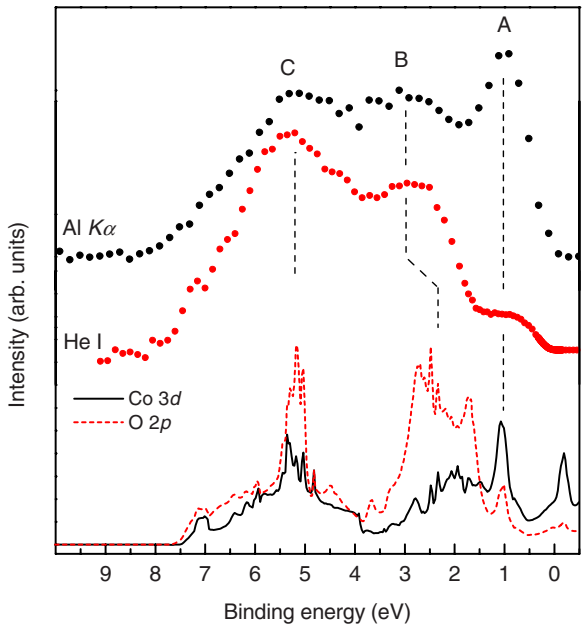

FIG. 6. (Color online) Experimental valence band spectra collected at room temperature using Al $K\alpha$ and He I radiations. The lines denote the calculated Co 3*d* and O 2*p* partial densities of states corresponding to the intermediate spin configuration of Co including spin-orbit coupling.

the intensities of features B and C become dominant in the He I spectrum. It is well known that the photoemission cross section is very sensitive to the excitation energies.[38] While the cross section of O 2*p* states is larger than that of Co 3*d* states in the He I spectrum, the relative cross section becomes opposite in the Al $K\alpha$ energies, making the cross section for Co 3*d* states significantly larger than that of O 2*p* states. In addition, PES is significantly surface sensitive at He I photon energies, while the Al $K\alpha$ spectrum represents largely the bulk contributions. Thus, the changes in intensity of various features due to the change in excitation energy are used to identify the dominant character of the features and the energy positions of the features in the Al $K\alpha$ spectrum are used as the representation of the bulk spectrum. The spectral evolution with the change in photon energy suggests that feature A is predominantly contributed by Co 3*d* states and features B and C have a large O 2*p* character. No significant feature is observed between 6 and 8 eV binding energies. This clearly suggests that the experimental results are very similar to the results obtained for IS configuration shown in Fig. 4(b).

In order to bring out clarity to this comparison, we plot the O 2*p* and Co 3*d* PDOSs corresponding to IS configuration in Fig. 6. The peak position of feature B is somewhat higher (0.5 eV) in the experimental spectra compared to the calculated results. Such small shift in the completely filled nonbonding O 2*p* bands has often been observed in the LDA results due to the underestimation of the electron correlation among the O 2*p* electrons.[27] The energy positions of features A and C in the experimental spectra and the large Co 3*d* character of feature A and O 2*p* character of feature C is revealed remarkably in the calculated results. Even the small shoulder in the binding energy range of 5.5–7.5 eV with relatively larger O 2*p* character is reproduced in the calculated results.

Moreover, the total energy for the IS state is found to be the lowest. The energy for LS state is about 762 meV/f.u. higher than that for the IS state. The calculation for the HS state could not be converged using normal procedure and hence we followed the "fixed spin moment method," as described by Korotin *et al.*[9] These results clearly suggest that the electronic structure of $LaCoO_3$ at room temperature corresponds primarily to the intermediate spin state configuration of Co and the contribution from HS state configuration may not be so significant. These results appear to be different from those in the recent studies based on cluster approximations.[21] Such difference may not be surprising as in the cluster calculations, the Co 3*d* and O 2*p* bands are approximated to atomic energy levels.

Finally, we investigate the applicability of *ab initio* band structure calculations in understanding the shallow core level spectrum. Such study will be quite interesting as the core-hole potential is known to influence the final states of the core level photoemission. The integral background subtracted experimental spectrum along with the calculated one is plotted in Fig. 7(a). Three distinct features are visible in the spectrum. The features at 16 and 18 eV binding energies correspond to spin-orbit split La 5*p* states as marked in the

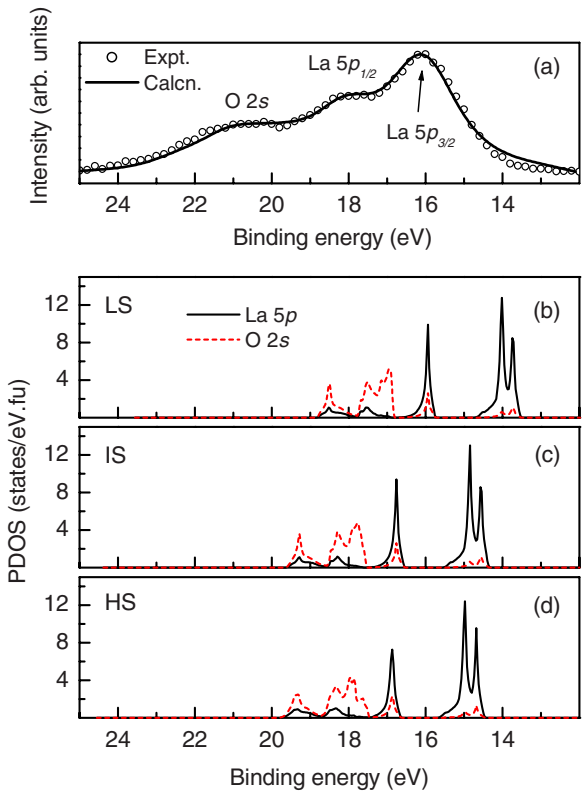

FIG. 7. (Color online) (a) Background subtracted La $5p$ and O $2s$ core level spectra (symbols) collected at room temperature. The solid line represents the spectrum simulated using PDOS corresponding to IS state configuration. La $5p$ (solid line) and O $2s$ (dashed line) PDOSs calculated using (b) LS, (c) IS, and (d) HS configurations of Co.

figure. The feature around 21 eV binding energy represent the signature of photoemission from O $2s$ levels.

We also show the La $5p$ and O $2s$ PDOSs corresponding to LS, IS, and HS configurations in different panels of Fig. 7. All the three features are present in the calculated results corresponding to LS, IS, and HS states. The shape of the bands in each region remains almost the same in each spin state. The spin-orbit splitting of the La $5p$ contributions in the PDOS is about 2 eV, as also observed in the experimental spectra. However, the peak position of the bands corresponding to LS state appears at binding energies lower by about 1 eV in comparison with energies corresponding to IS and HS states, which are closer to the experimental spectra.

In order to simulate the experimental spectrum, we have shifted the calculated O $2s$ and La $5p$ PDOSs obtained from IS configuration by 3.1 and 1.2 eV, respectively. Such deviation in energy position of the experimental and calculated spectra is expected in LMTO band structure calculations. It is well known that the LMTO basis set makes use of a Taylor series expansion in energy about the center of gravity of the occupied band (E_ν). As a result, the calculated density of states is most accurate close to E_ν but becomes less accurate at energies far from E_ν. Thus, one expects deviation in the energy of calculated and experimental La $5p$ and O $2s$ bands. On general ground, such deviation for La $5p$ and O $2s$ bands may not be the same. In addition, correlation effects among these electrons are also not considered in the calculations. Such correlation is also known to affect the energy of the core level spectra.

The shifted O $2s$ and La $5p$ PDOSs are then multiplied by photoemission cross sections of the corresponding states.[38] Resulting La $5p$ and O $2s$ PDOSs are convoluted with Lorentzians having full widths at half maximum (FWHM) of 1.8 and 1.4 eV, respectively, to account for the lifetime broadening and a Gaussian having FWHM of 0.6 eV to account for the resolution broadening. The simulated spectrum is shown by a solid line overlapped on the experimental spectrum in Fig. 7(a). The reproduction of the experimental spectrum is remarkable. It is noted here that these calculations cannot create features appearing due to different screening effects expected in the final state of photoemission. Almost perfect reproduction of the experimental spectrum in the present case indicates that final state effects may not be significant in the case of O $2s$ and La $5p$ photoemission. This suggests that one can employ band structure calculations to determine the shallow core level spectra of O and A site atoms in the ABO_3 structure. The absence of features corresponding to final state effect due to different screening (poorly screened, well screened, etc.) of the core hole in the O $2s$ and La $5p$ spectra may not be surprising. In the case of O $2s$ photoemission, the screening of the core hole due to charge transfer may be negligible as the O $2p$ band is almost filled. In the case of La $5p$ photoemission too, such effect is expected to be small as the unoccupied bands corresponding to La appear much above the Fermi level. Thus, these results suggest that one can study the crystal structure induced evolution of the electronic structure using such spectra, which can also be determined using *ab initio* band structure calculations.

IV. CONCLUSIONS

In summary, we have investigated the electronic structure of $LaCoO_3$ at room temperature using various forms of *ab initio* calculations and high-resolution photoemission spectroscopy on high quality single crystal. We observe that GGA+U calculations provide a good description of the ground state. Spin-orbit coupling appears to play a significant role in the case of IS and HS states of Co, which is most pronounced in the case of IS state of Co. The calculated Co $3d$ and O $2p$ partial densities of states corresponding to the intermediate spin state of Co provide the best description of the experimental valence band spectra at room temperature. This suggests that the spin state of Co at room temperature presumably has a dominant intermediate spin configuration and that the contribution from high spin state is not so significant at this temperature. The applicability of the *ab initio* band structure calculations in understanding the shallow core level spectrum is also studied. The calculated spin-orbit splitting of La $5p$ states is found to be about 2 eV,

which is identical to the experimentally observed splitting. The line shape of the calculated spectrum provides a good description of the experimental spectrum. This suggests that final state effects may not be significant in the case of O 2*s* and La 5*p* photoemission in $LaCoO_3$.

ACKNOWLEDGMENTS

The authors would like to thank A. V. Narlikar for continued support. S. Patil is thankful to CSIR, India, for financial support.

[1] J. B. Goodenough, J. Phys. Chem. Solids **6**, 287 (1958).
[2] R. R. Heikes, R. C. Miller, and R. Mazelsky, Physica (Amsterdam) **30**, 1600 (1964).
[3] P. M. Raccah and J. B. Goodenough, Phys. Rev. **155**, 932 (1967).
[4] V. G. Bhide, D. S. Rajoria, and Y. S. Reddy, Phys. Rev. Lett. **28**, 1133 (1972).
[5] B. W. Veal and D. J. Lam, J. Appl. Phys. **49**, 1461 (1978).
[6] M. Abbate, J. C. Fuggle, A. Fujimori, L. H. Tjeng, C. T. Chen, R. Potze, G. A. Sawatzky, H. Eisaki, and S. Uchida, Phys. Rev. B **47**, 16124 (1993).
[7] S. R. Barman and D. D. Sarma, Phys. Rev. B **49**, 13979 (1994).
[8] D. J. Lam, B. W. Veal, and D. E. Ellis, Phys. Rev. B **22**, 5730 (1980).
[9] M. A. Korotin, S. Yu. Ezhov, I. V. Solovyev, V. I. Anisimov, D. I. Khomskii, and G. A. Sawatzky, Phys. Rev. B **54**, 5309 (1996).
[10] V. P. Plakhty, P. J. Brown, B. Grenier, S. V. Shiryaev, S. N. Barilo, S. V. Gavrilov, and E. Ressouche, J. Phys.: Condens. Matter **18**, 3517 (2006).
[11] S. Yamaguchi, Y. Okimoto, H. Taniguchi, and Y. Tokura, Phys. Rev. B **53**, R2926 (1996).
[12] Y. Kobayashi, N. Fujiwara, S. Murata, K. Asai, and H. Yasuoka, Phys. Rev. B **62**, 410 (2000).
[13] C. Zobel, M. Kriener, D. Bruns, J. Baier, M. Grüninger, T. Lorenz, P. Reutler, and A. Revcolevschi, Phys. Rev. B **66**, 020402(R) (2002).
[14] P. G. Radaelli and S. W. Cheong, Phys. Rev. B **66**, 094408 (2002).
[15] G. Maris, Y. Ren, V. Volotchaev, C. Zobel, T. Lorenz, and T. T. M. Palstra, Phys. Rev. B **67**, 224423 (2003).
[16] I. A. Nekrasov, S. V. Streltsov, M. A. Korotin, and V. I. Anisimov, Phys. Rev. B **68**, 235113 (2003).
[17] A. Ishikawa, J. Nohara, and S. Sugai, Phys. Rev. Lett. **93**, 136401 (2004).
[18] D. Phelan, D. Louca, S. Rosenkranz, S.-H. Lee, Y. Qiu, P. J. Chupas, R. Osborn, H. Zheng, J. F. Mitchell, J. R. D. Copley, J. L. Sarrao, and Y. Moritomo, Phys. Rev. Lett. **96**, 027201 (2006).
[19] T. Saitoh, T. Mizokawa, A. Fujimori, M. Abbate, Y. Takeda, and M. Takano, Phys. Rev. B **55**, 4257 (1997).
[20] K. Knízek, Z. Jirák, J. Hejtmánek, and P. Novák, J. Phys.: Condens. Matter **18**, 3285 (2006).
[21] M. W. Haverkort, Z. Hu, J. C. Cezar, T. Burnus, H. Hartmann, M. Reuther, C. Zobel, T. Lorenz, A. Tanaka, N. B. Brookes, H. H. Hsieh, H.-J. Lin, C. T. Chen, and L. H. Tjeng, Phys. Rev. Lett. **97**, 176405 (2006).
[22] A. Podlesnyak, S. Streule, J. Mesot, M. Medarde, E. Pomjakushina, K. Conder, A. Tanaka, M. W. Haverkort, and D. I. Khomskii, Phys. Rev. Lett. **97**, 247208 (2006).
[23] D. Prabhakaran, A. T. Boothroyd, F. R. Wondre, and T. J. Prior, J. Cryst. Growth **275**, e827 (2005).
[24] S. Y. Savrasov, Phys. Rev. B **54**, 16470 (1996); arXiv:cond-mat/0409705 (unpublished).
[25] S. H. Vosko, L. Wilk, and M. Nusair, Can. J. Phys. **58**, 1200 (1980).
[26] J. P. Perdew, K. Burke, and M. Ernzerhof, Phys. Rev. Lett. **77**, 3865 (1996).
[27] D. D. Sarma, N. Shanthi, S. R. Barman, N. Hamada, H. Sawada, and K. Terakura, Phys. Rev. Lett. **75**, 1126 (1995).
[28] Kalobaran Maiti, Phys. Rev. B **73**, 115119 (2006).
[29] K. Maiti and R. S. Singh, Phys. Rev. B **71**, 161102(R) (2005).
[30] S. K. Pandey, Ashwani Kumar, S. M. Chaudhari, and A. V. Pimpale, J. Phys.: Condens. Matter **18**, 1313 (2006).
[31] S. K. Pandey, S. Khalid, and A. V. Pimpale, J. Phys.: Condens. Matter **19**, 036212 (2007).
[32] A. Chainani, M. Mathew, and D. D. Sarma, Phys. Rev. B **46**, 9976 (1992).
[33] T. Arima, Y. Tokura, and J. B. Torrance, Phys. Rev. B **48**, 17006 (1993).
[34] E. Iguchi, K. Ueda, and W. H. Jung, Phys. Rev. B **54**, 17431 (1996).
[35] T. Hotta, Rep. Prog. Phys. **69**, 2061 (2006).
[36] T. Mizokawa, L. H. Tjeng, G. A. Sawatzky, G. Ghiringhelli, O. Tjernberg, N. B. Brookes, H. Fukazawa, S. Nakatsuji, and Y. Maeno, Phys. Rev. Lett. **87**, 077202 (2001).
[37] H. Wu, Z. Hu, D. I. Khomskii, and L. H. Tjeng, Phys. Rev. B **75**, 245118 (2007).
[38] J. J. Yeh and I. Lindau, At. Data Nucl. Data Tables **32**, 1 (1985).